EFFECT OF MASS LOADING ON BOW SHOCK NEBULAE

Giovanni Morlino

Purdue University, INDIANA
CNRS/APC, Paris, FRANCE

In collaboration with:
M. Lyutikov & M. Vorster

Workshop on Relativistic Plasma Astrophysics

Purdue University May 12-15 2014

SN 1006
NASA/ESA/Hubble Heritage Team
(STScI/AURA)

Structure of bow-shock nebula

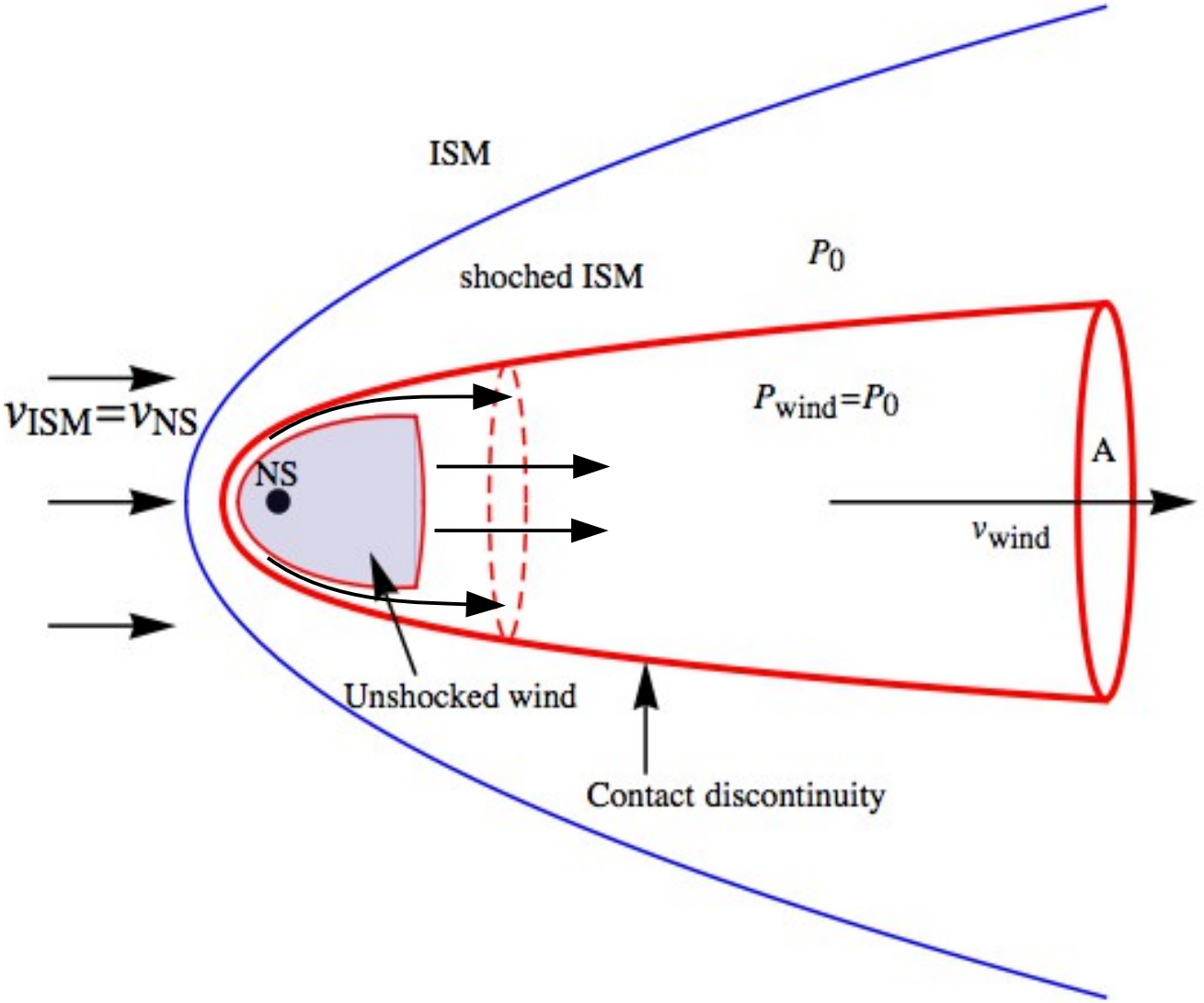

Structure of bow-shock nebula

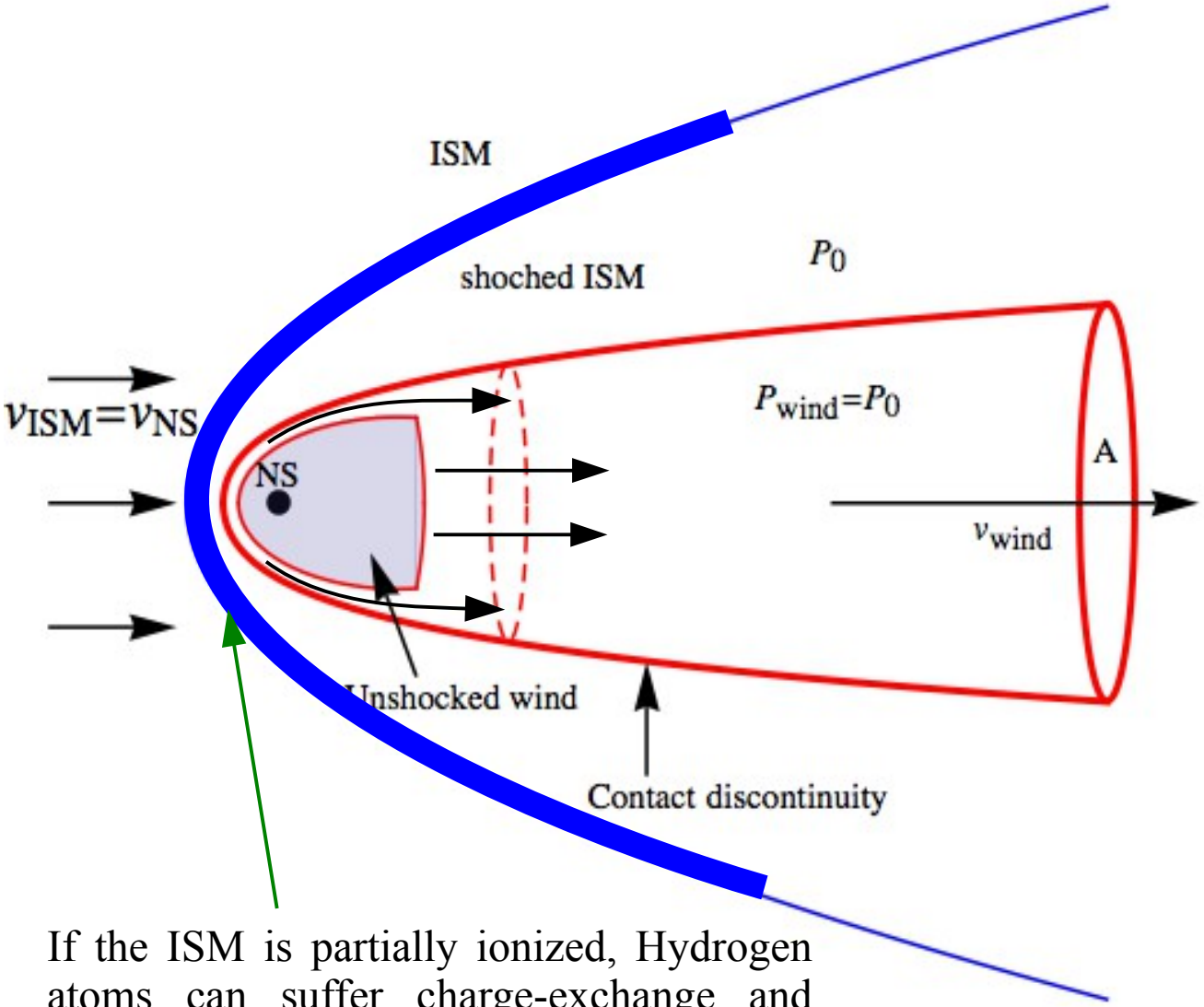

If the ISM is partially ionized, Hydrogen atoms can suffer charge-exchange and collisional excitation emitting Balmer lines

Structure of bow-shock nebula

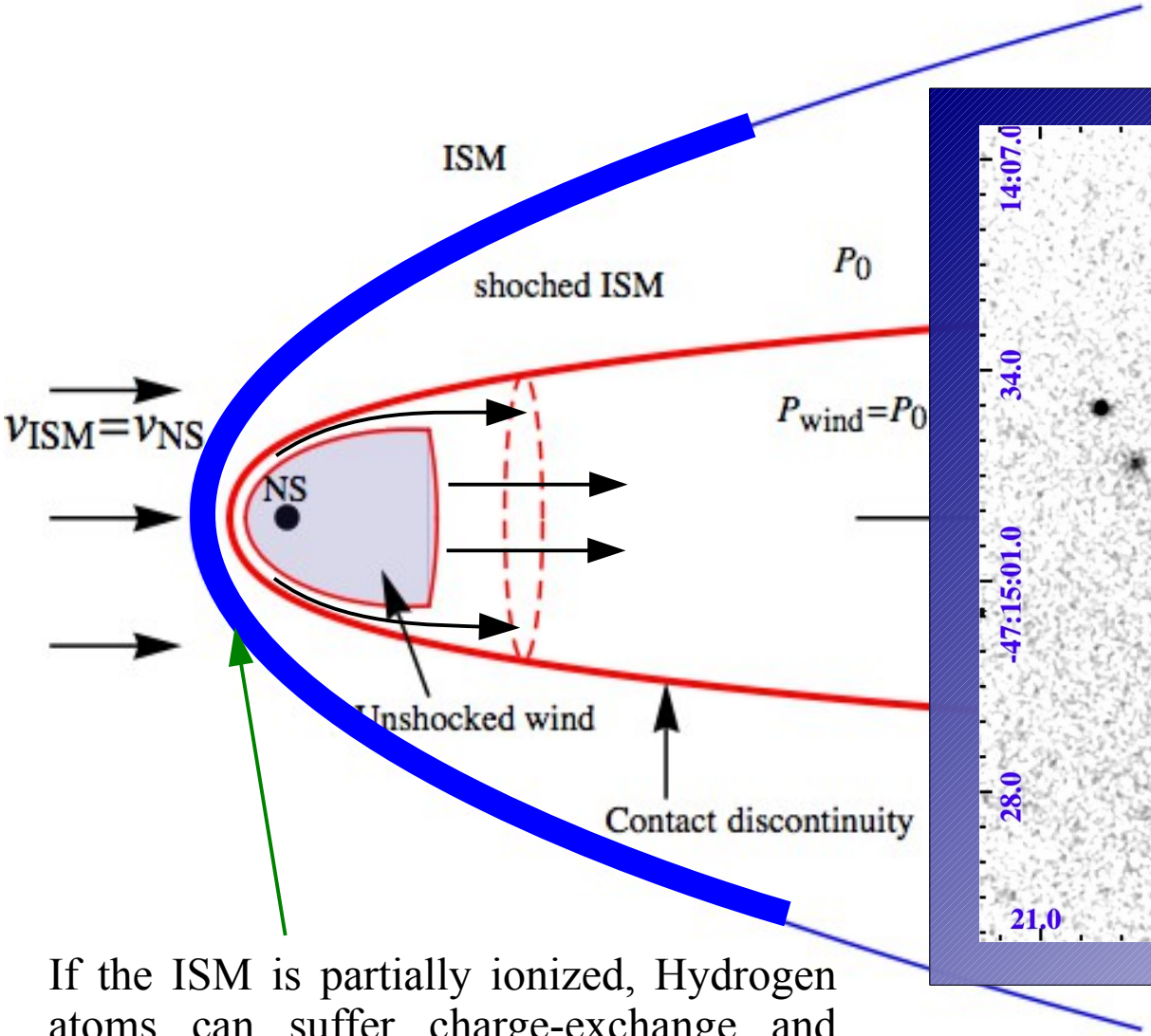

Hα emission from J0437-4714

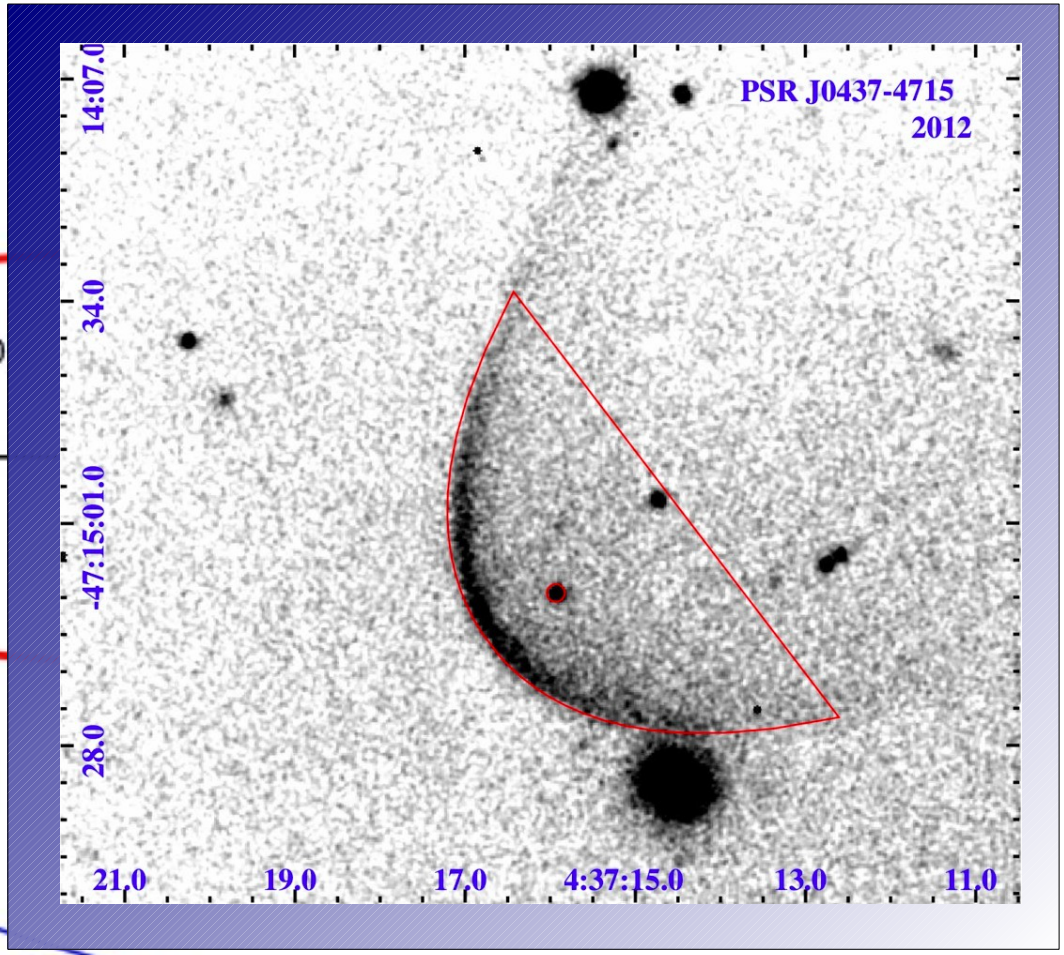

If the ISM is partially ionized, Hydrogen atoms can suffer charge-exchange and collisional excitation emitting Balmer lines

Structure of bow-shock nebula: simulations

[From Bucciantini, Amato & del Zanna 2005, *A&A* 434,189]

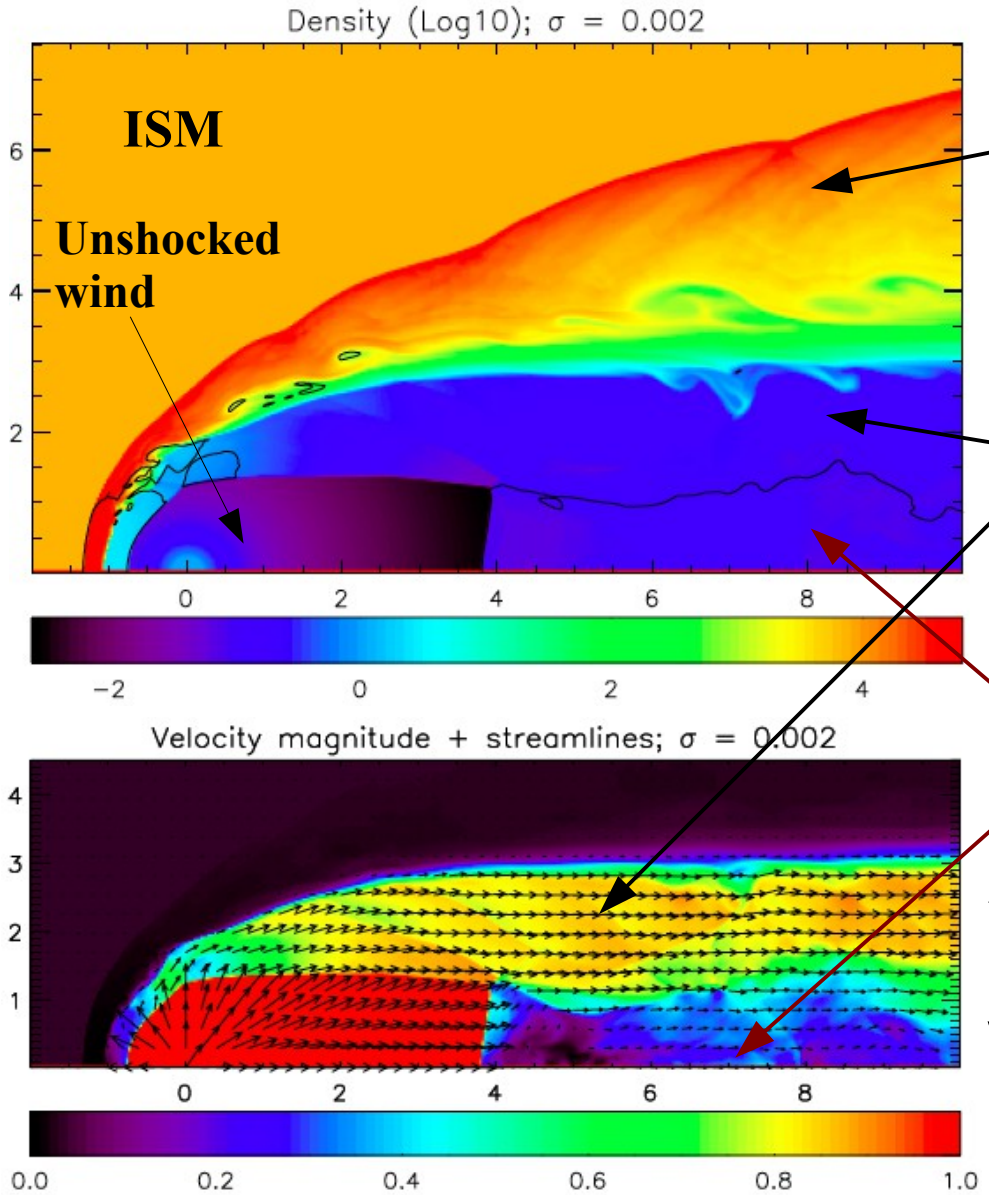

Summary of pulsar with Hα bow shock

[From Brownsberger & Romani 2014, arXiv:1402.5465]

- 6 over 9 known Hα bow shock nebulae show rapid expansion and/or contraction of the tale
- These features are axisymmetric along the propagation axes of the pulsar

This suggest that the tale could be modified by internal dynamics rather than by external effects (non uniform ISM)

Cometary shape

OLD

NEW

Pulsar	$\dot{E}^a_{34}$ erg/s	Lgτ y	d^b kpc	μ_T mas/y	F^c_γ 10^{-11}	$F^c_{x,NT}$ 10^{-13}	θ_a $''$	$F_{a\mathrm{H}\alpha}$ $\gamma/\mathrm{cm}^2/\mathrm{s}$
J0437−4715	0.55	9.8	0.16 P	141.3	1.67	7.9	9.3	6.7E-3
J0742−2822	19.0	5.2	2.0 D	29.0	1.72	<0.2	1.4	1.8E-4
J1509−5850	68.2	5.2	2.6 D		12.70	3.0	1.2	1.4E-4
J1741−2054	12.6	5.6	0.38 D		11.70	2.0	2.3	4.6E-3
J1856−3754	3.E-4	6.5	0.16 P	332.0	–	0.0	0.85	3.E-5
J1959+2048	21.9	9.5	2.5 D	30.4	1.7	0.7	3.6	1.8E-3
J2030+4415	2.90	5.8	0.9 G		5.8	2.8	1.1	1.8E-3
J2124−3358	0.68	9.8	0.30 P	52.7	3.7	0.8	5.0	5.3E-4
J2225+6535	0.16	6.1	1.86 D 1.00	182.0	–	0.0	0.12	3.6E-5

Guitar nebula (powered by PRS B2224+65)

[From Gautam A. et al. 2013]

From Palomar Observatory (1995)

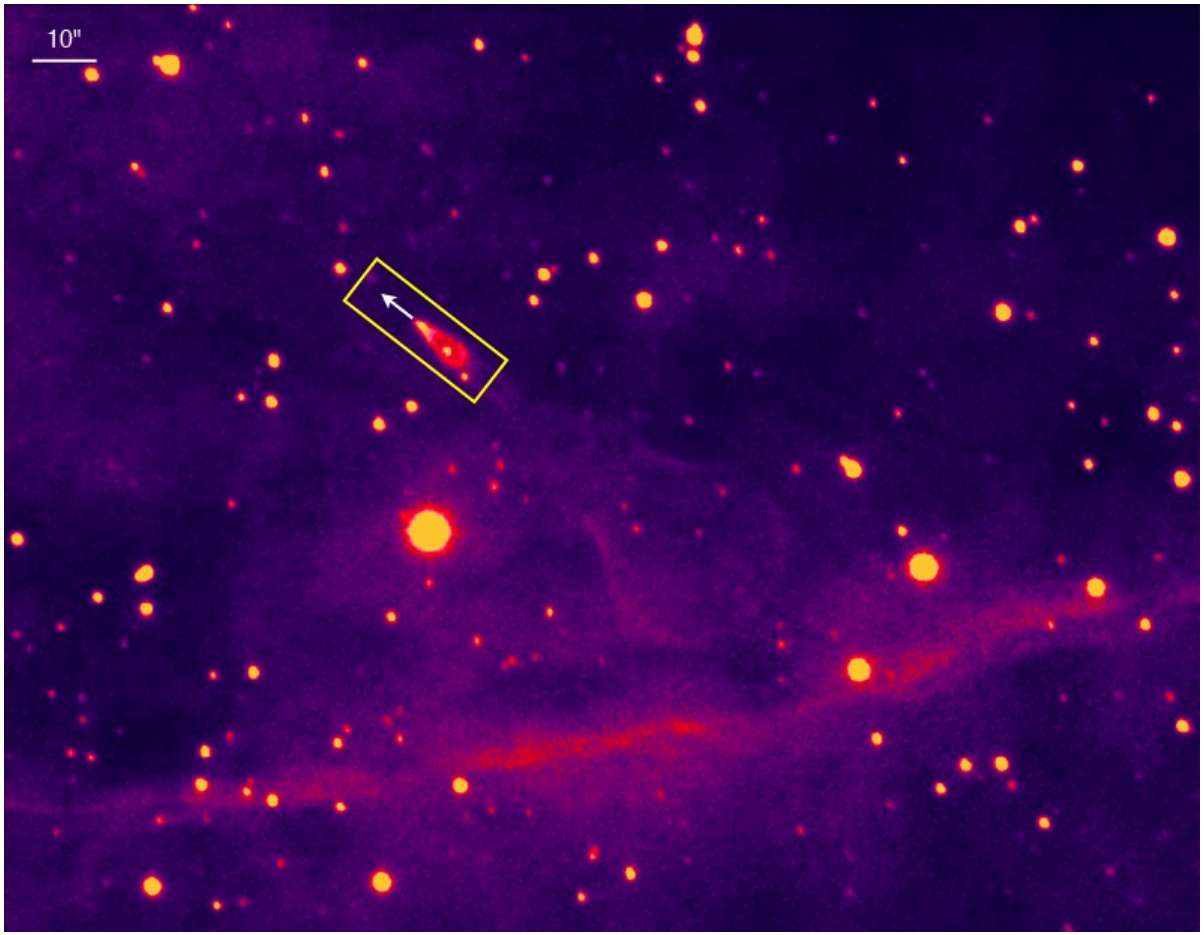

Guitar nebula (powered by PRS B2224+65)

[From Gautam A. et al. 2013]

Balmer emission: images from HST

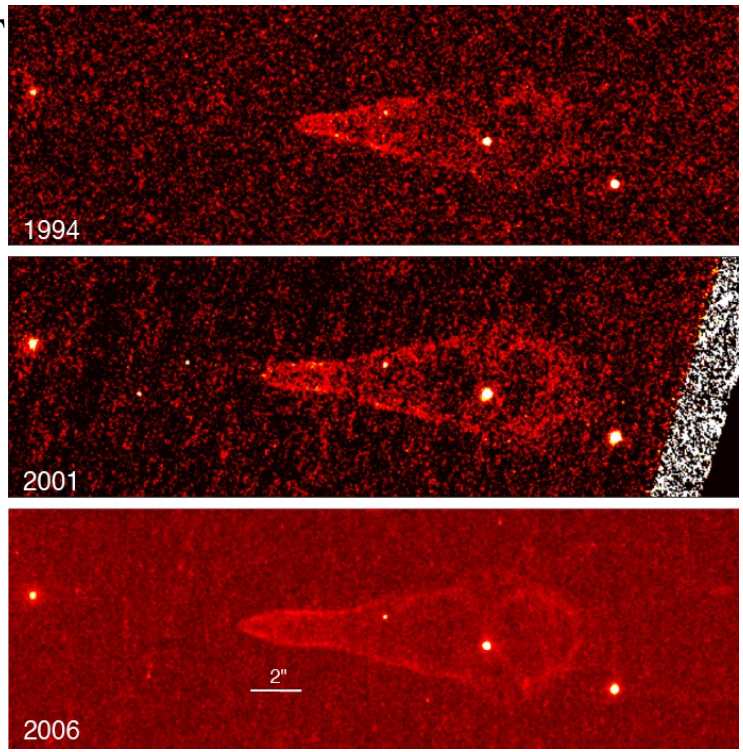

From Palomar Observatory (1995)

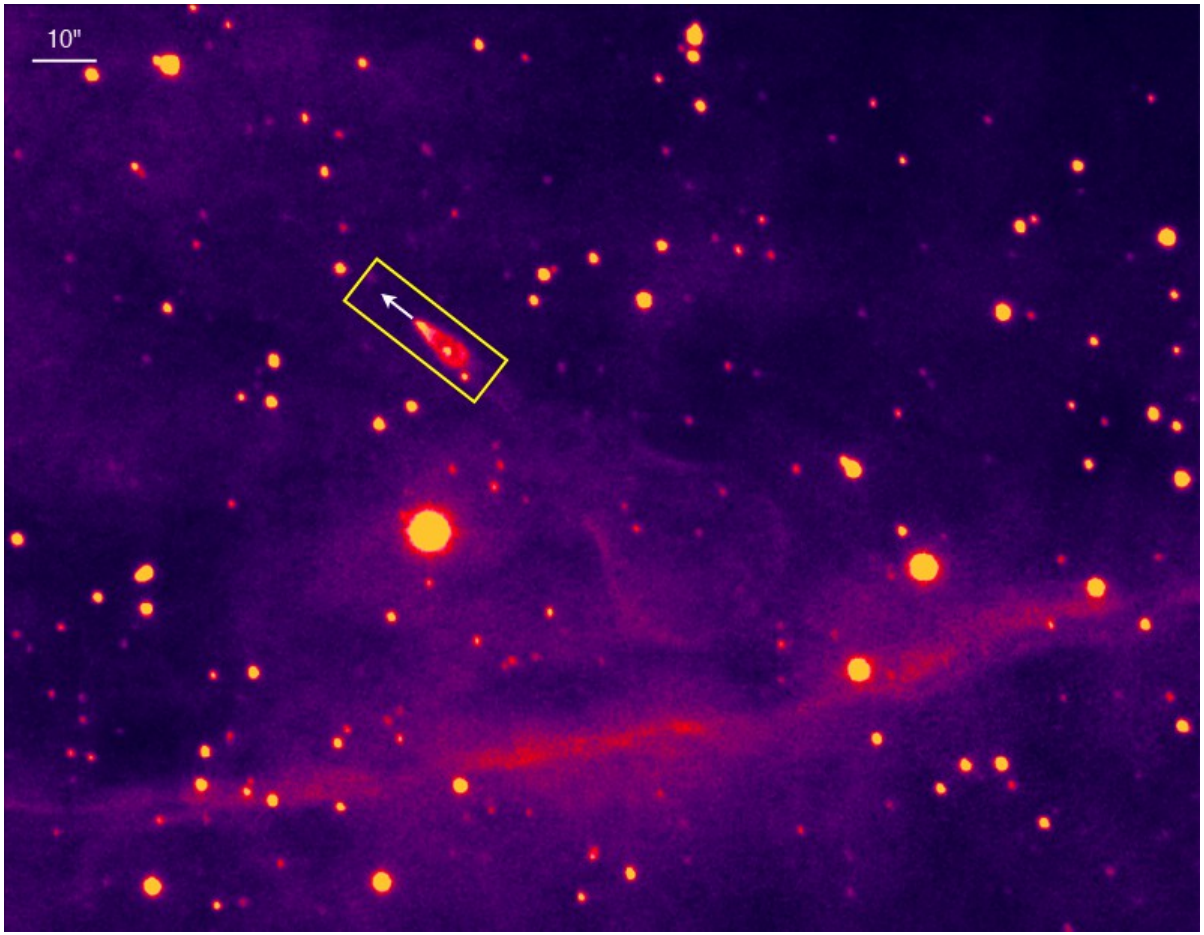

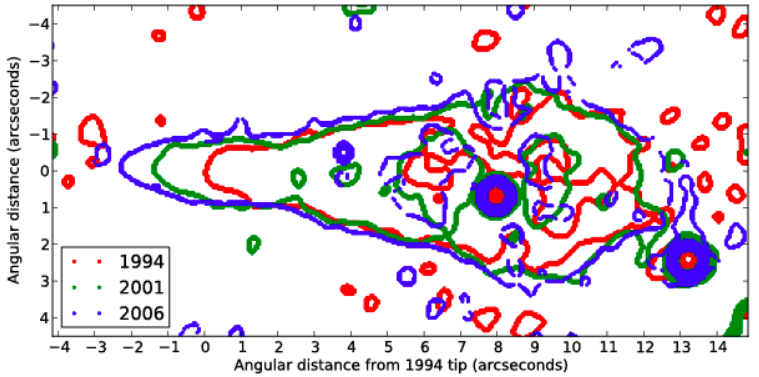

PSR J2124-3358

[From Brownsberger & Romani 2014, *ApJ* accepted arXiv:1402.5465]

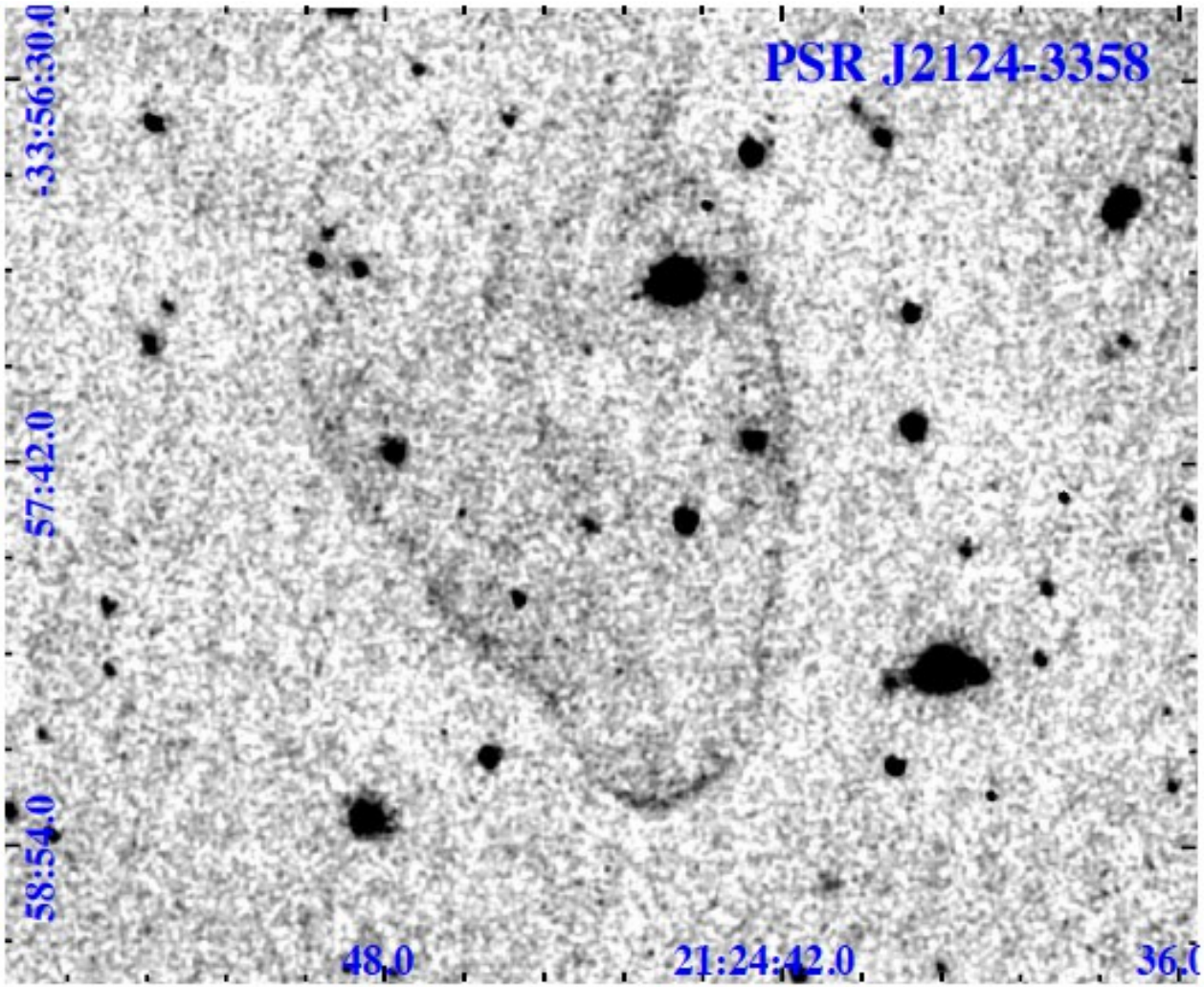

PSR J2124-3358

[From Brownsberger & Romani 2014, *ApJ* accepted arXiv:1402.5465]

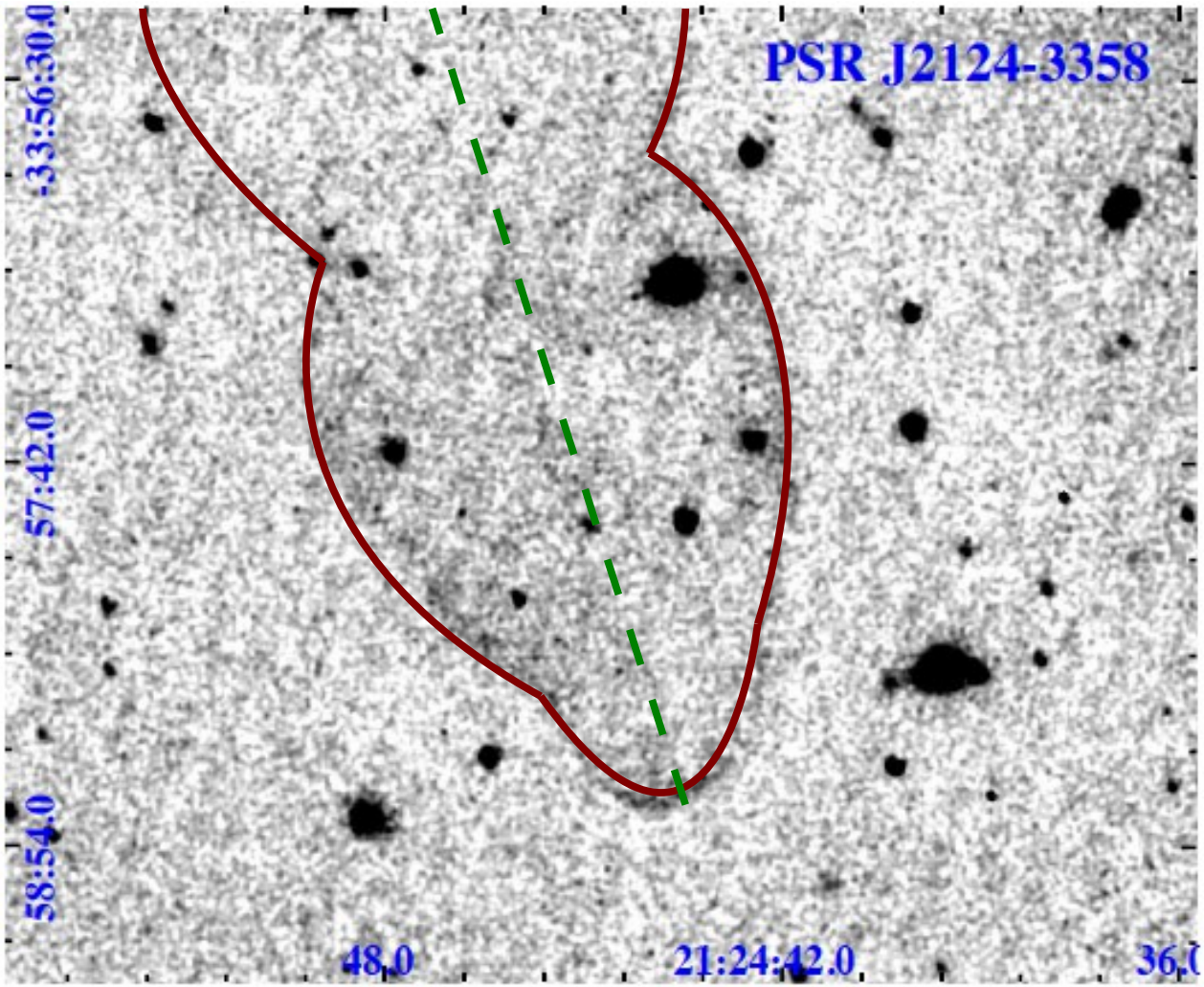

PSR J2124-3358

[From Brownsberger & Romani 2014, *ApJ* accepted arXiv:1402.5465]

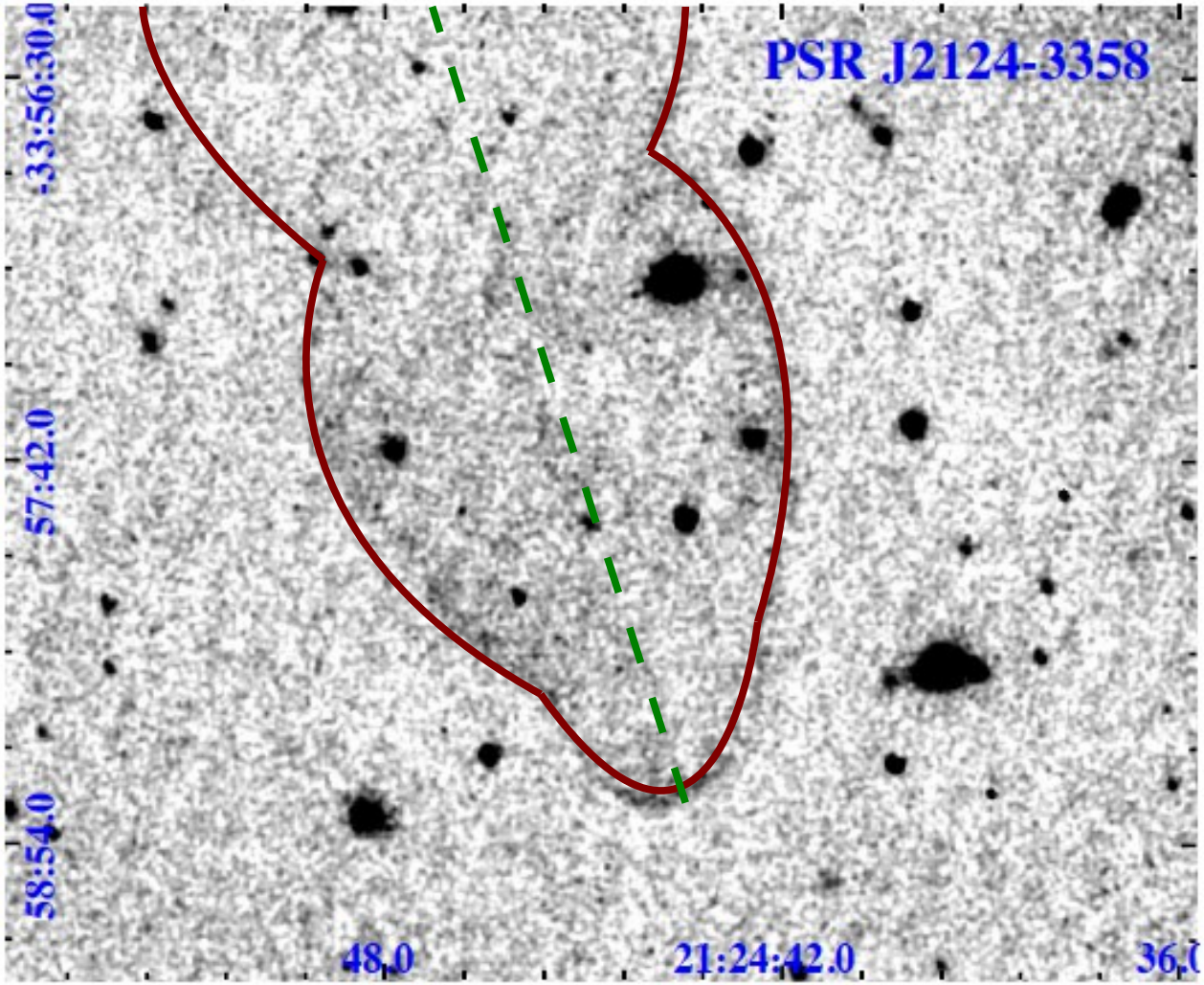

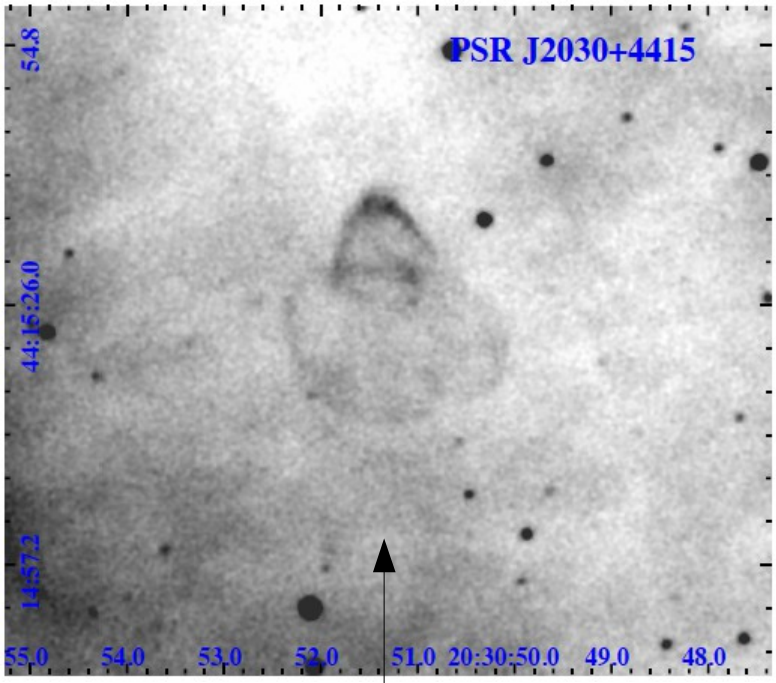

New discovered with a survey for Hα bow shock emission around nearby FermiLAT γ-detected energetic pulsars

PSR J0742-2822

[From Brownsberger & Romani 2014, *ApJ* accepted arXiv:1402.5465]

Hα image with background star light subtracted

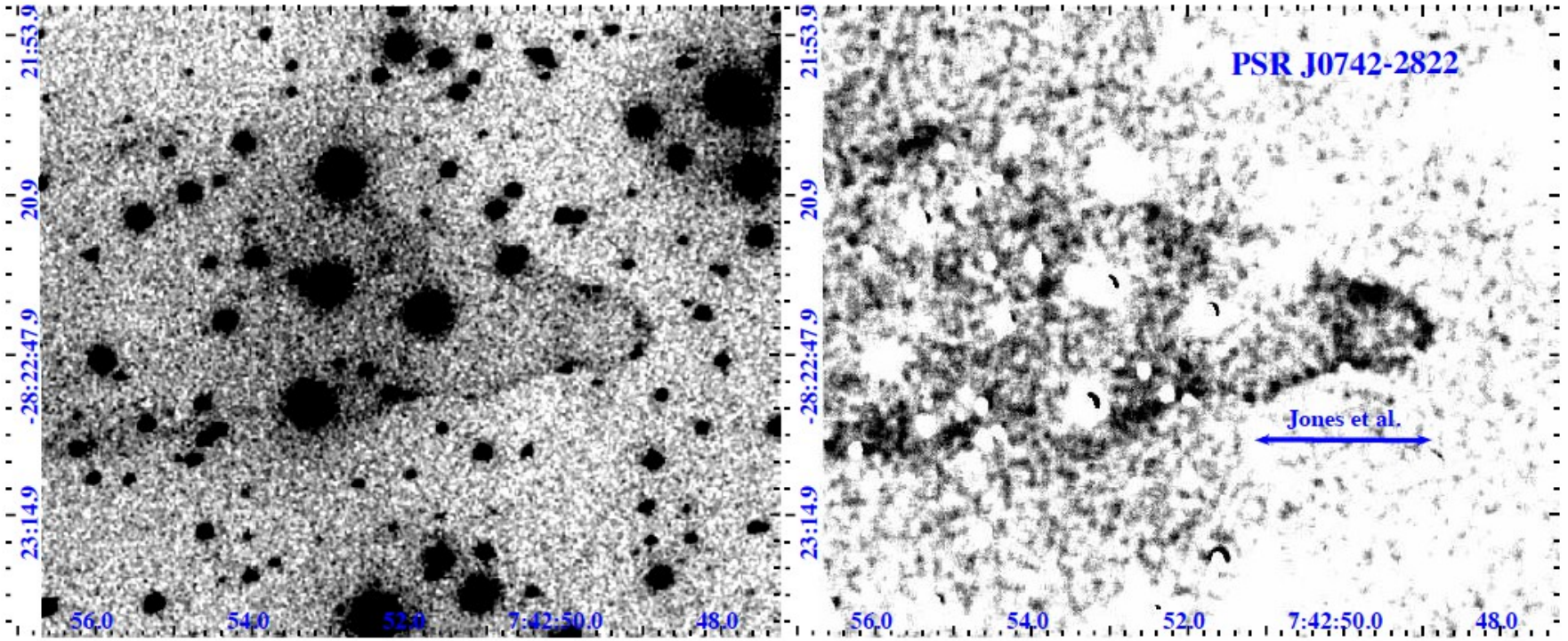

PSR J1509-5850

[From Brownsberger & Romani 2014, *ApJ* accepted arXiv:1402.5465]

New discovered!

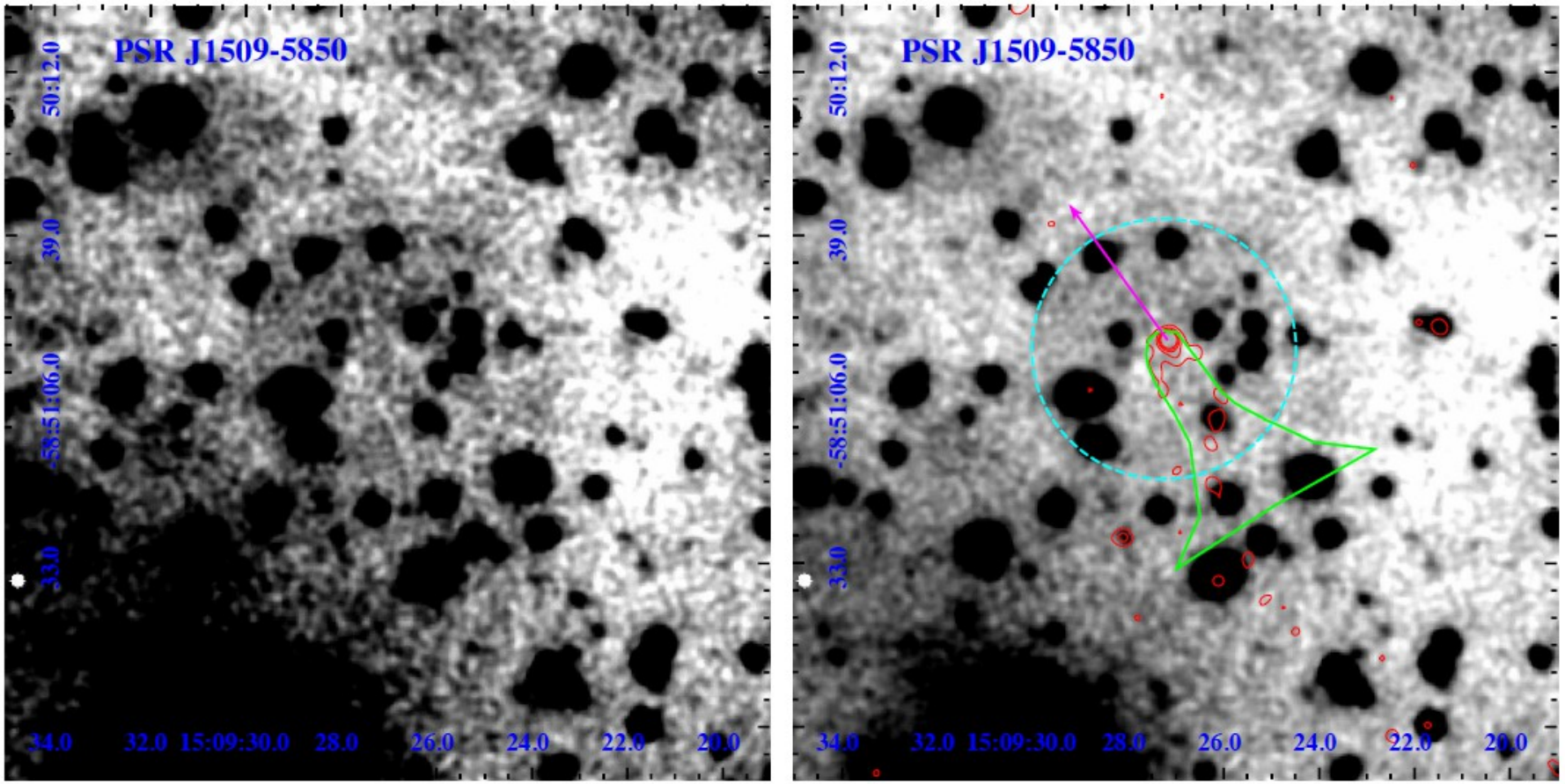

Left: a median-filtered 3 Å~ 600 W012 SOI image of PSR J0742−2822, smoothed with a 0.45″ Gaussian. The *right panel* shows an image with a scaled continuum (W014) image subtracted and 0.9″ top-hat smoothing. The arrow indicates extent of the previous nebula detection.

Two bow shock nebulae in X-rays

[From Kargaltsev, O. et al 2008, *ApJ* 684, 542]

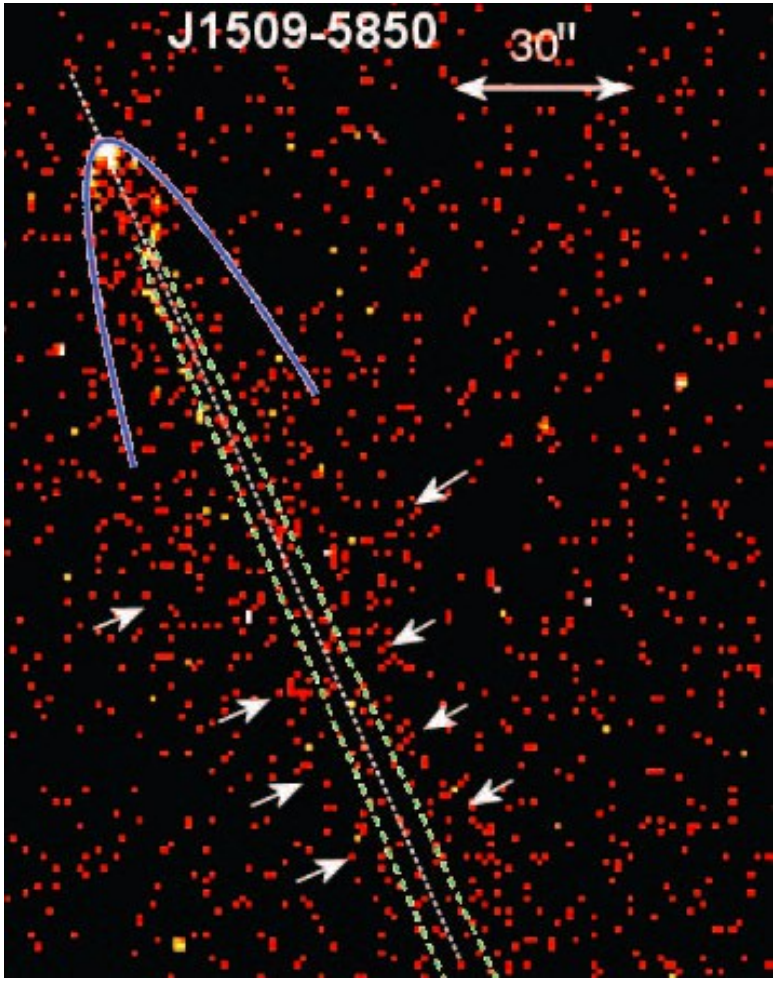

J1509 tail (in the 1–7 keV band, binned to the pixel size of 200). The blue line shows an approximate boundary of the PWN head within 15" from the pulsar, but it does not fit the tail's shape at larger distances. The white arrows show an approximate observed width of the tail.

Two bow shock nebulae in X-rays

[From Kargaltsev, O. et al 2008, *ApJ* 684, 542]

The Mushroom PWN powered by PSR B0355+54. Notice the sudden narrowing (transition from the “cap" to the “stem")

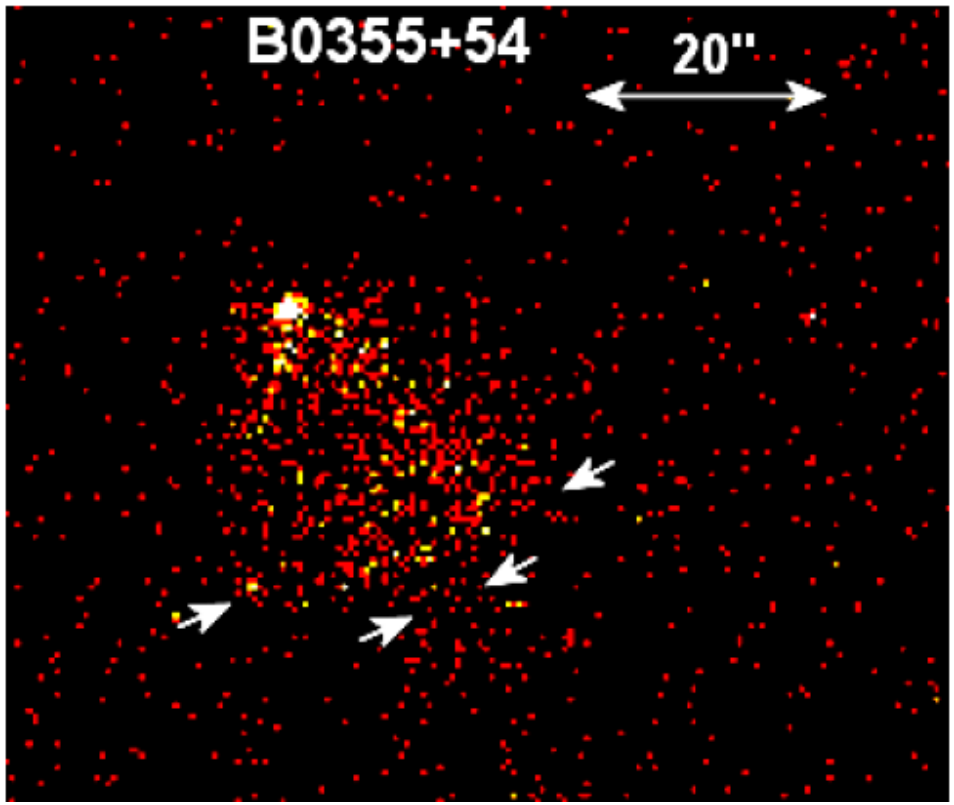

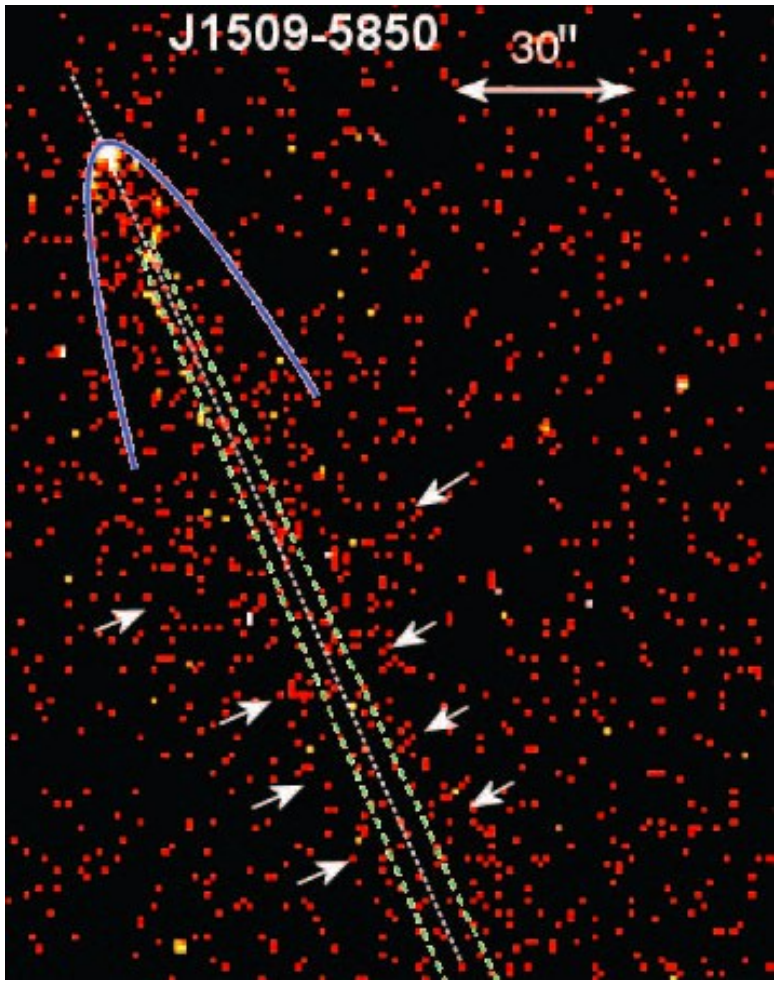

J1509 tail (in the 1–7 keV band, binned to the pixel size of 200). The blue line shows an approximate boundary of the PWN head within 15" from the pulsar, but it does not fit the tail’s shape at larger distances. The white arrows show an approximate observed width of the tail.

Interaction length-scales for neutrals

$$d_S = \left(\frac{L_{wind}}{4\pi v_{NS}^2 \rho_0 c} \right)^{1/2} = 2.5 \cdot 10^{15} \left(\frac{L_{wind}}{10^{34} erg} \right)^{1/2} \left(\frac{V_{NS}}{500\, km/s} \right) \left(\frac{n_0}{cm^{-3}} \right)^{-1/2} cm$$

Stagnation distance

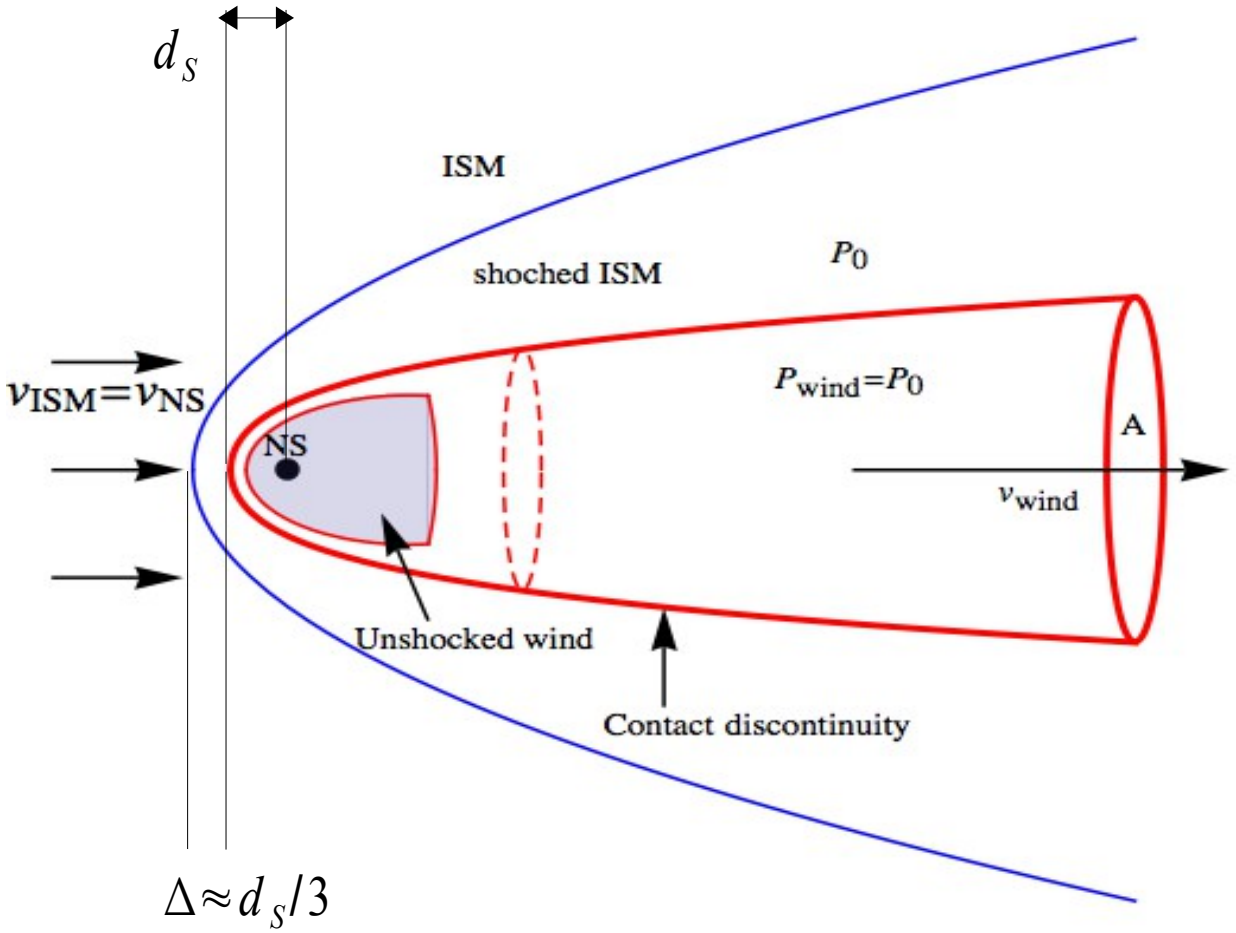

Interaction length-scales for neutrals

$$d_S = \left(\frac{L_{wind}}{4\pi v_{NS}^2 \rho_0 c} \right)^{1/2} = 2.5 \cdot 10^{15} \left(\frac{L_{wind}}{10^{34} erg} \right)^{1/2} \left(\frac{V_{NS}}{500\, km/s} \right) \left(\frac{n_0}{cm^{-3}} \right)^{-1/2} cm$$

Stagnation distance

$$\lambda_{coll} = \frac{V_{NS}}{x_{ion} n_{ISM} \langle \sigma_{coll} v_{rel} \rangle} \rightarrow \begin{cases} \lambda_{CE} = 1.3 \cdot 10^{15} \ cm \sim d_S \\ \lambda_{ion} = 7.0 \cdot 10^{18} \ cm \gg d_S \end{cases}$$

Collisional length-scale in the shocked ISM

Neutral Hydrogen from the ISM can easily penetrate into the wind region

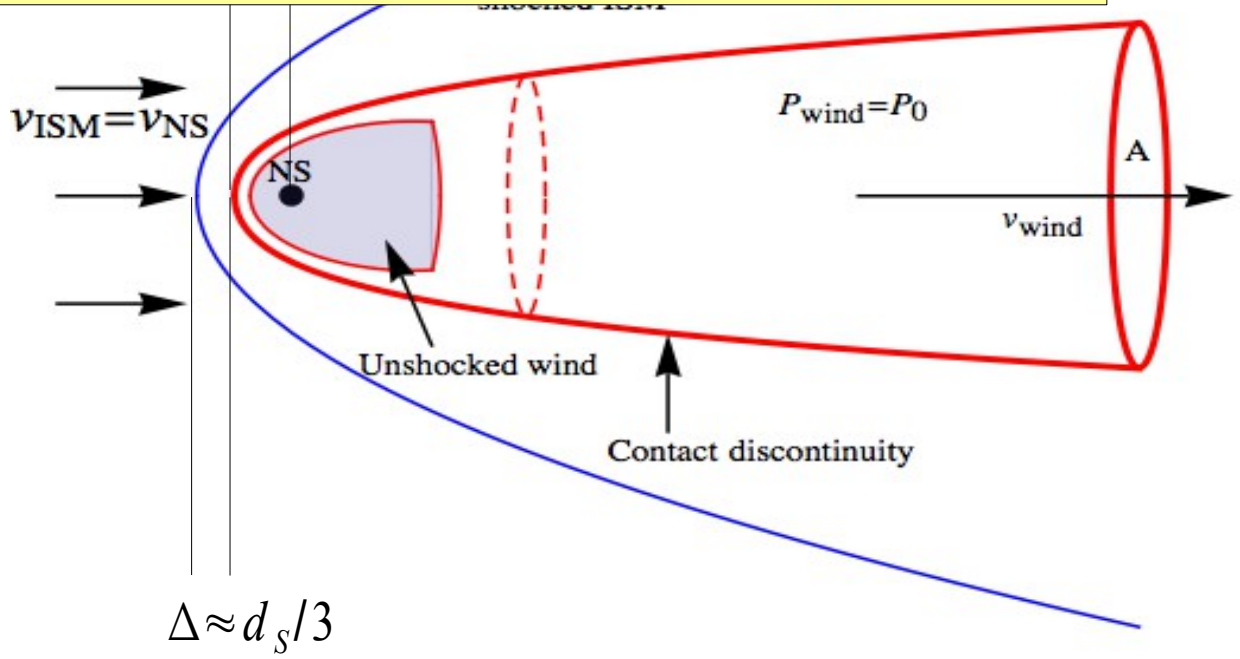

$\Delta \approx d_S/3$

Interaction length-scales for neutrals

$$d_S = \left(\frac{L_{wind}}{4\pi v_{NS}^2 \rho_0 c} \right)^{1/2} = 2.5 \cdot 10^{15} \left(\frac{L_{wind}}{10^{34} erg} \right)^{1/2} \left(\frac{V_{NS}}{500\, km/s} \right) \left(\frac{n_0}{cm^{-3}} \right)^{-1/2} cm$$

Stagnation distance

$$\lambda_{coll} = \frac{V_{NS}}{x_{ion} n_{ISM} \langle \sigma_{coll} v_{rel} \rangle} \rightarrow \begin{cases} \lambda_{CE} = 1.3 \cdot 10^{15} \ cm \sim d_S \\ \lambda_{ion} = 7.0 \cdot 10^{18} \ cm \gg d_S \end{cases}$$

Collisional length-scale in the shocked ISM

Neutral Hydrogen from the ISM can easily penetrate into the wind region

$$\dot{M}_{pulsar} = \frac{L_w}{\gamma_w c^2} = n_e m_e \pi d_S^2 c \rightarrow n_e \approx 10^{-10}$$

Electron-positron density inside the wind

$$\lambda_{ion,wind} = \frac{V_{NS}}{n_e \sigma_{Bethe} c} \approx 7 \cdot 10^{23} \left(\frac{V_{SN}}{500\, km/s} \right) \left(\frac{n_e}{10^{-10} cm^{-3}} \right)^{-1} cm$$

Ionization scale of hydrogen inside the wind

$\Delta \approx d_S / 3$

Interaction length-scales for neutrals

$$d_S = \left(\frac{L_{wind}}{4\pi v_{NS}^2 \rho_0 c}\right)^{1/2} = 2.5\cdot 10^{15}\left(\frac{L_{wind}}{10^{34} erg}\right)^{1/2}\left(\frac{V_{NS}}{500\, km/s}\right)\left(\frac{n_0}{cm^{-3}}\right)^{-1/2} cm$$

Stagnation distance

$$\lambda_{coll} = \frac{V_{NS}}{x_{ion} n_{ISM} \langle \sigma_{coll} v_{rel} \rangle} \rightarrow \begin{cases} \lambda_{CE} = 1.3\cdot 10^{15}\ cm \sim d_S \\ \lambda_{ion} = 7.0\cdot 10^{18}\ cm \gg d_S \end{cases}$$

Collisional length-scale in the shocked ISM

Neutral Hydrogen from the ISM can easily penetrate into the wind region

$$\dot{M}_{pulsar} = \frac{L_w}{\gamma_w c^2} = n_e m_e \pi d_S^2 c \rightarrow n_e \approx 10^{-10}$$

Electron-positron density inside the wind

$$\lambda_{ion,wind} = \frac{V_{NS}}{n_e \sigma_{Bethe} c} \approx 7\cdot 10^{23}\left(\frac{V_{SN}}{500\, km/s}\right)\left(\frac{n_e}{10^{-10} cm^{-3}}\right)^{-1} cm$$

Ionization scale of hydrogen inside the wind

$$\lambda_{load} = \lambda_{ion,wind}\frac{\rho_{wind}}{\rho_N} = \frac{V_{NS}}{(1-x_{ion}) n_{ISM} \sigma_{Bethe} c}\frac{m_e}{m_p} \approx 10^{16}\ cm$$

Distance where mass loaded density = wind density

Our mathematical approach

- Stationary approach
- Single fluid (non relativistic)
- Quasi 1-D along the propagation direction z
- No magnetic field

$$\frac{\partial}{\partial z}\left[\rho_w v_w A_w\right] = \phi_N$$

$$\frac{\partial}{\partial z}\left[\left(\rho_w v_w^2 + P_w\right) A_w\right] = \phi_N v_{NS}$$

$$\frac{\partial}{\partial z}\left[\left(\frac{1}{2}\rho_w v_w^2 + \frac{\gamma_w}{\gamma_w - 1} P_w\right) v_w A_w\right] = \frac{1}{2}\phi_N v_{NS}^3$$

MASS FLUX

MOMENTUM FLUX

ENERGY FLUX

Conservation equation along the flux tube for a stationary system

$$\phi_N = \rho_N \rho_w \frac{\langle \sigma_{ion} v \rangle}{m_e} A_w$$

RATE OF MASS LOADING

$P_N = 0$ — Cold neutral fluid

$\langle \sigma_{ion} v \rangle_{f_w(v)} = const$ — Constant ionization rate

$$P_w = P_0$$

PRESURE EQUILIBRIUM BETWEEN WIND AND SHOCK ISM

Analytical solution

Coupled 1st order differential equations for flow speed and sound speed:

$$\frac{\partial v_w}{\partial \eta} = -\frac{1}{2}\,\frac{v_w\left(v_w - V_{NS}\right)}{v_w^2 - c_s^2}\,\left[v_w(\gamma+1) - V_{NS}(\gamma-1)\right]$$

$$\frac{\partial c_s}{\partial \eta} = \frac{c_s}{2\,v_w}\left[\frac{\partial v_w}{\partial \eta}\left(1-\gamma\frac{v_w^2}{c_s^2}\right) - \gamma\frac{v_w\left(v_w - V_{NS}\right)}{c_s^2} - 1\right]$$

If $v_{w,1} > V_{NS}$ and $M_1 \gtrless 1$ $\Rightarrow$ $\frac{\partial v_w}{\partial \eta} \lessgtr 0$, $\frac{\partial c_s}{\partial \eta} \gtrless 0$ $\Rightarrow$ $M \searrow \nearrow$, $A \nearrow \searrow$

Solution for the flow cross-section:

$$A(\eta) = A_0 \exp\left[-\gamma \int_0^{\eta} \frac{v_w\left(\partial_\eta v_w + 1\right) - V_{NS}}{c_s^2}\, d\eta'\right]$$

$$\eta = \frac{z}{\lambda_{load}} = \frac{z}{\lambda_{ion}}\,\frac{\rho_N}{\rho_{wind,1}}$$

Moreover:

$$M \to 1 \quad \Rightarrow \quad \frac{\partial v_w}{\partial \eta} \to \mp\infty \quad \Rightarrow \quad \frac{\partial A}{\partial \eta} \to \pm\infty$$

Expansion velocity > sound speed
→ stationary approach no more valid

Results

Initial supersonic flow

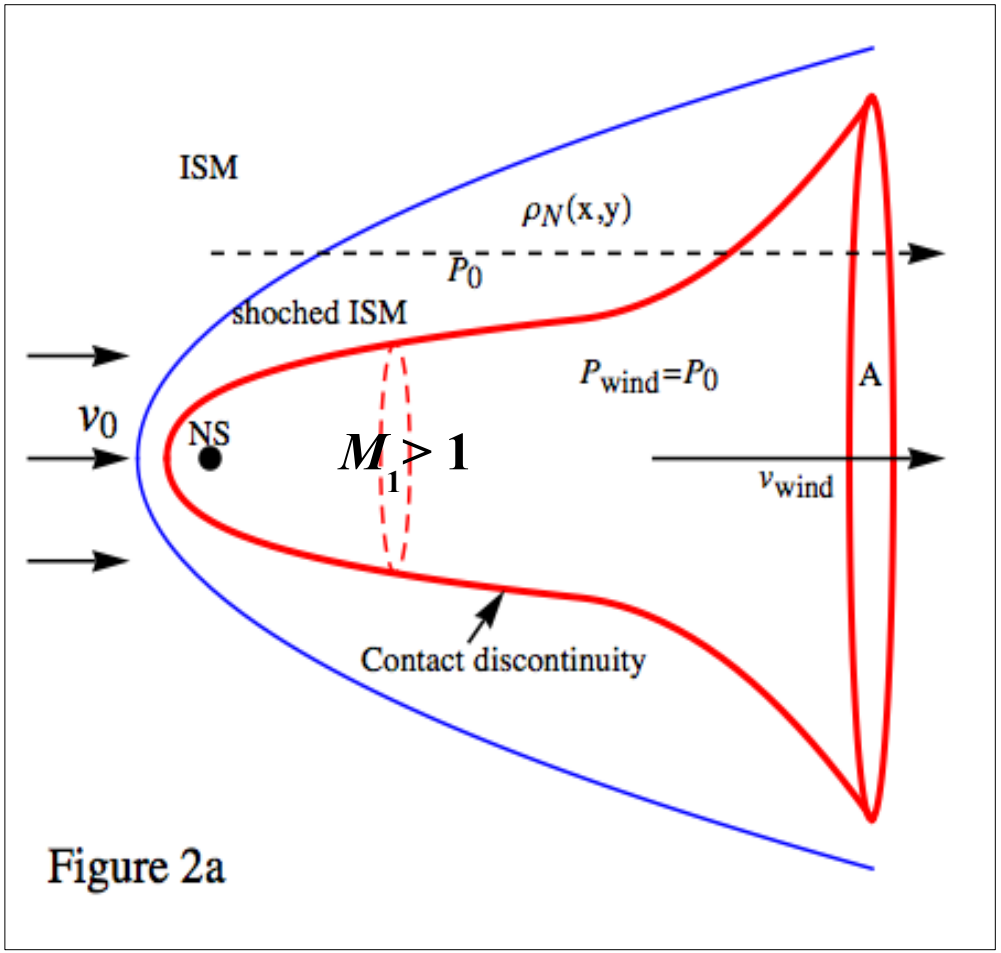

Figure 2a

Initial subsonic flow

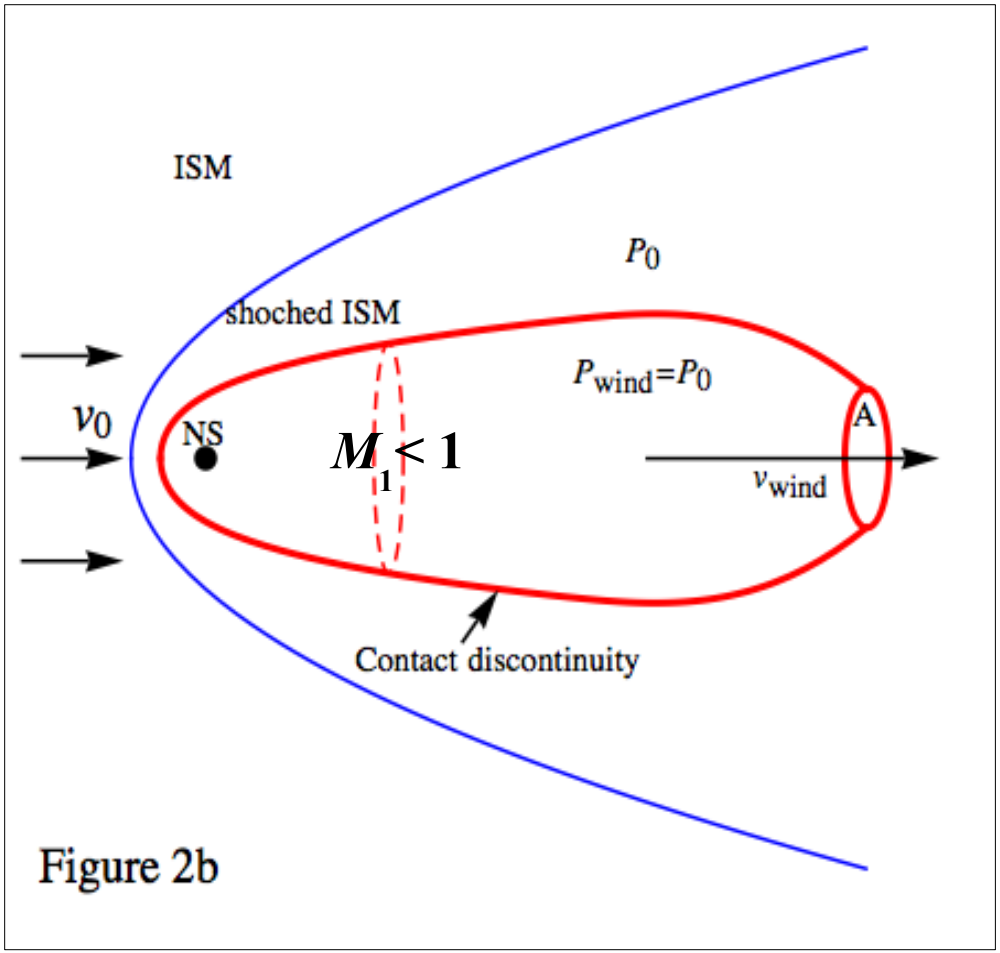

Figure 2b

Results

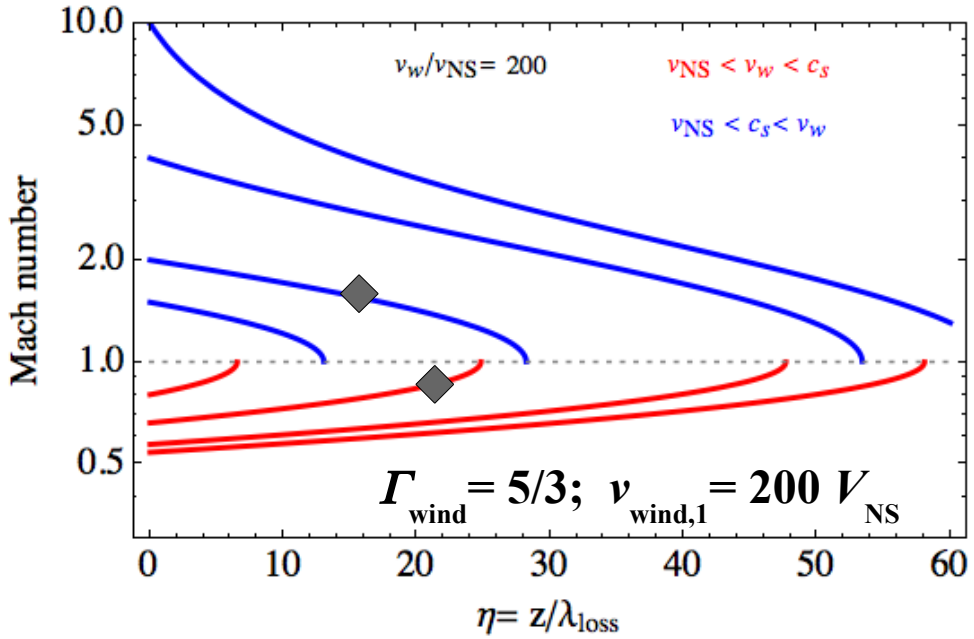
v_w/v_{NS}= 200
$v_{NS} < v_w < c_s$
$v_{NS} < c_s < v_w$
Mach number
$\Gamma_{wind} = 5/3;\ v_{wind,1} = 200\ V_{NS}$
$\eta = z/\lambda_{loss}$

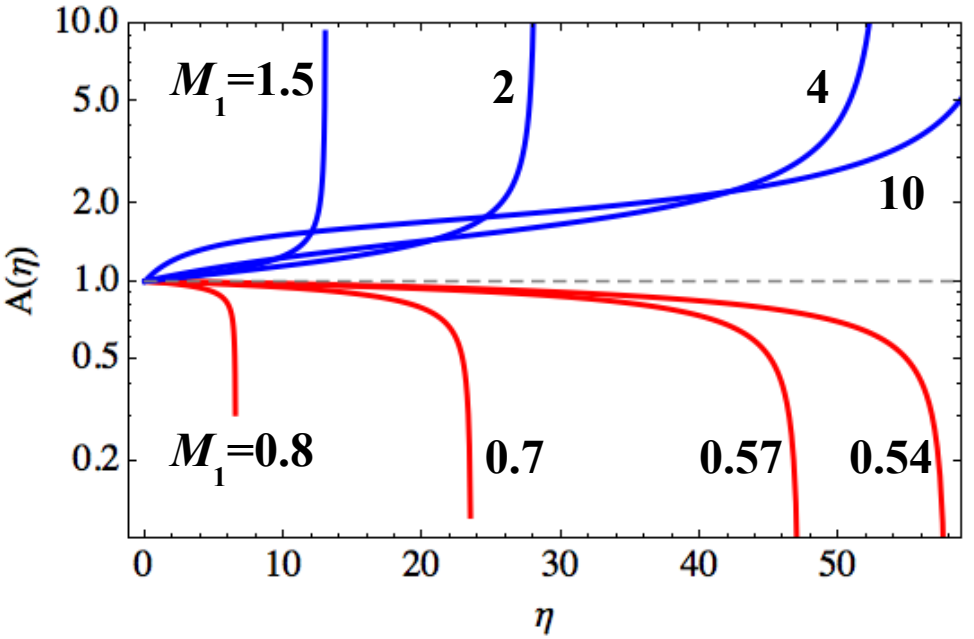
M_1=1.5
2
4
10
M_1=0.8
0.7
0.57
0.54
A(η)
η

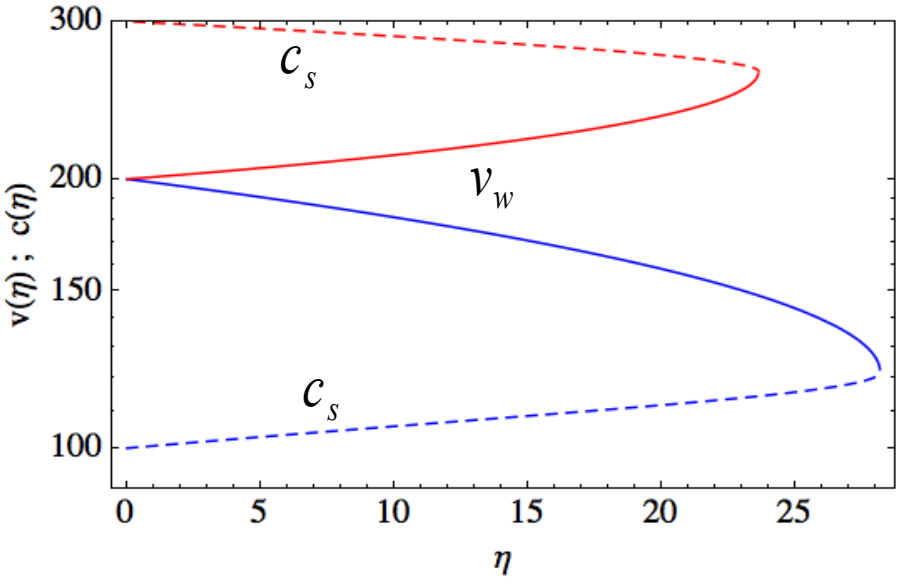
c_s
v_w
c_s
v(η) ; c(η)
η

Results

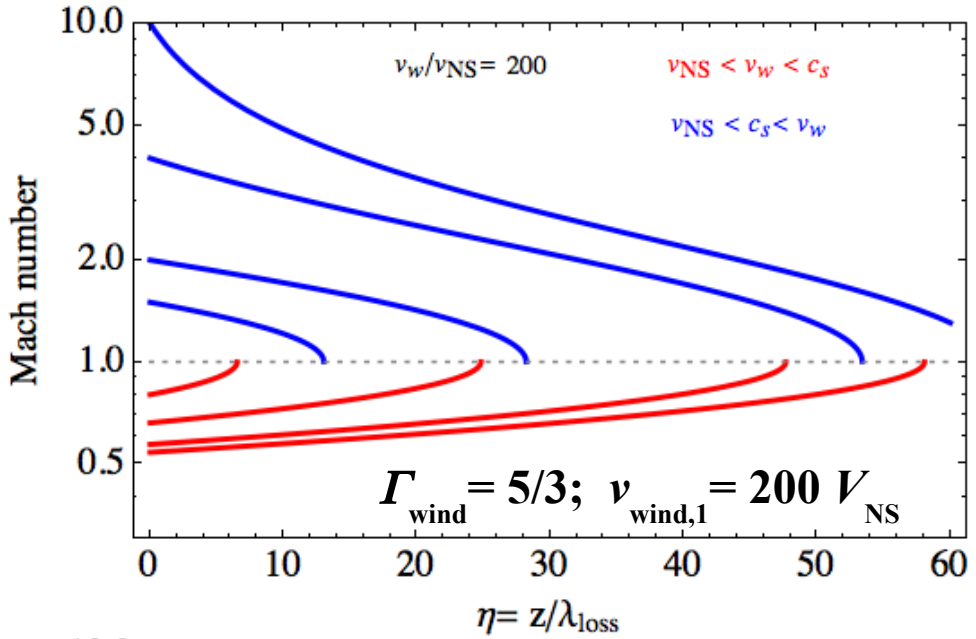
v_w/v_{NS}= 200
$v_{NS} < v_w < c_s$
$v_{NS} < c_s < v_w$
Mach number
$\Gamma_{wind} = 5/3;\ v_{wind,1} = 200\ V_{NS}$
$\eta = z/\lambda_{loss}$

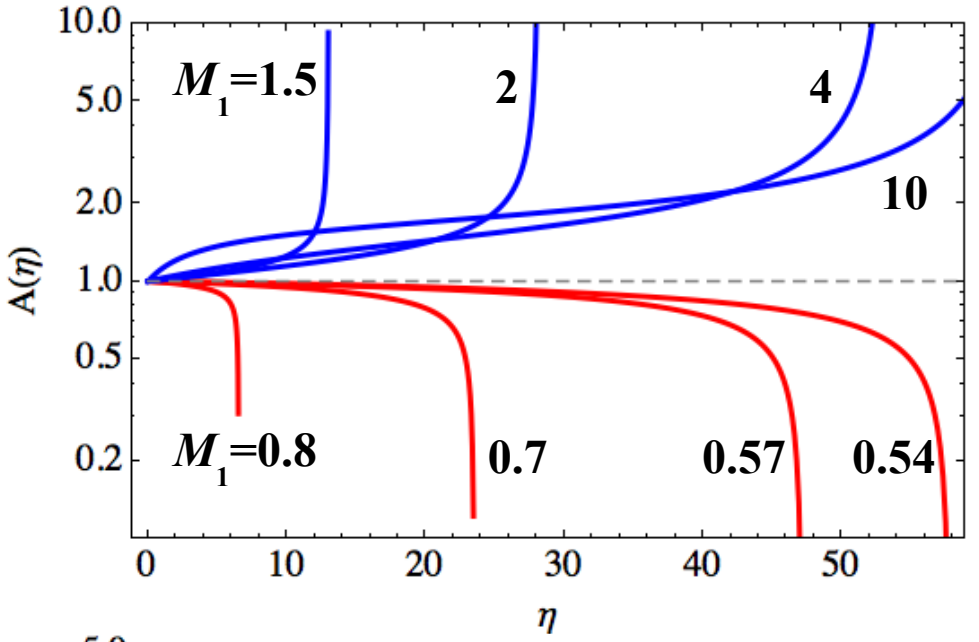
M_1=1.5
2
4
10
M_1=0.8
0.7
0.57
0.54
A(η)
η

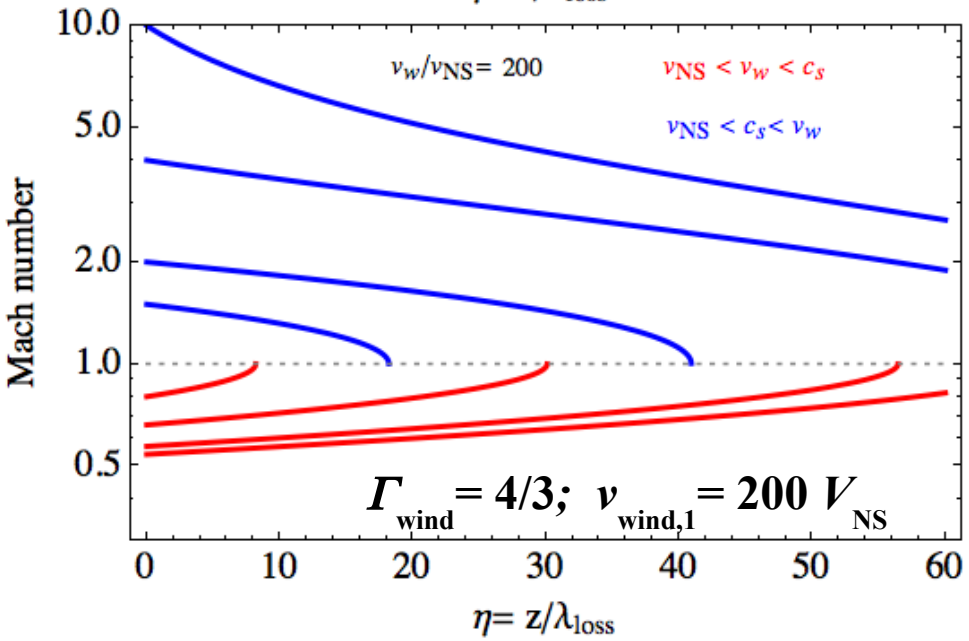
v_w/v_{NS}= 200
$v_{NS} < v_w < c_s$
$v_{NS} < c_s < v_w$
Mach number
$\Gamma_{wind} = 4/3;\ v_{wind,1} = 200\ V_{NS}$
$\eta = z/\lambda_{loss}$

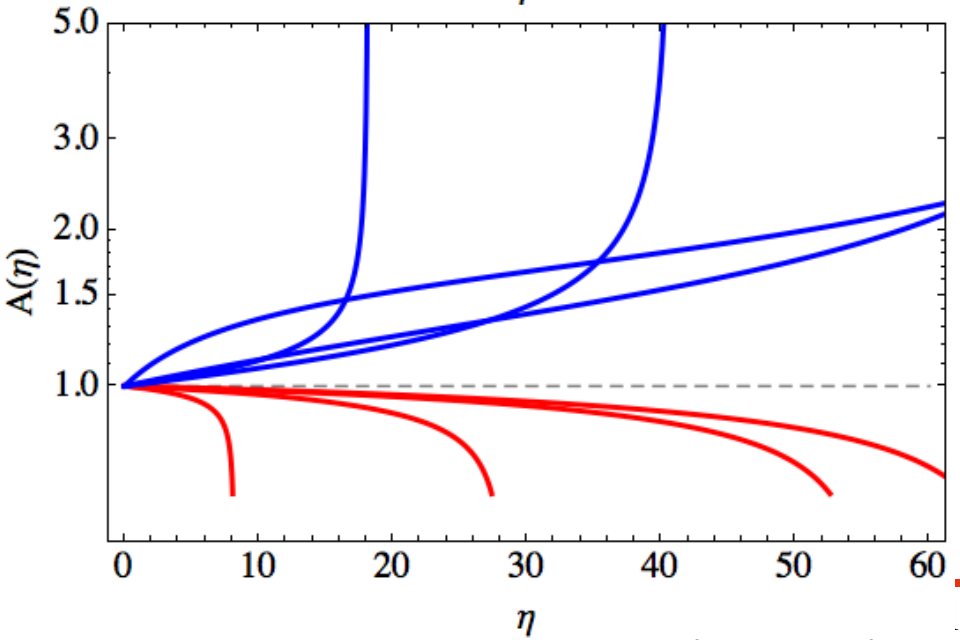
A(η)
η

CONCLUSIONS

- **Neutral Hydrogen from ISM can easily penetrate into the relativistic wind of bow-shock pulsar wind nebulae**

- **Internal dynamics of the wind can be strongly affected by neutrals on the typical mass loading scale**
  - ***Mach > 1 → the flow slows down and expands***
  - ***Mach < 1 → the flow accelerates and contracts***

- **Present results can explain the shape observed in many bow shock nebulae observed in Balmer emission (and X-rays)**

- **The stationary approach fails when M → 1**
  Simulations are needed to get a comprehensive time dependent solution and to include magnetic field

Results

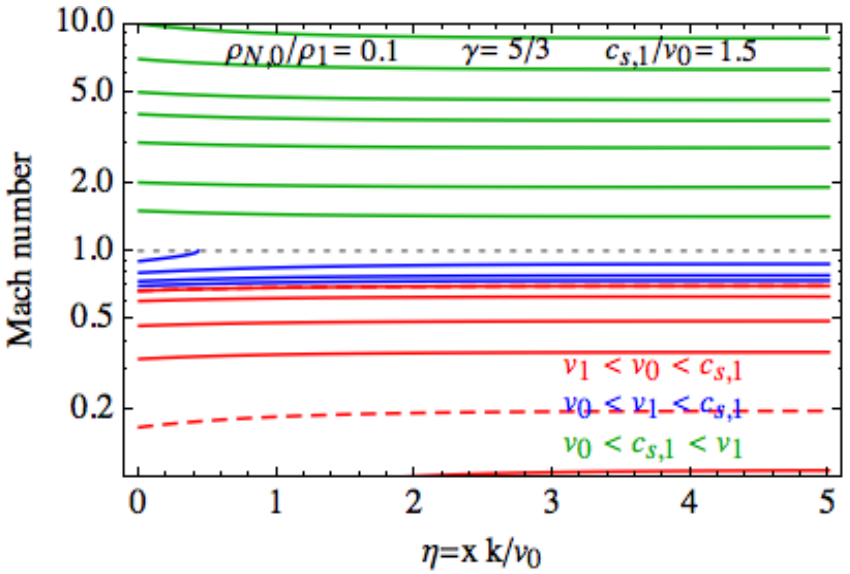
$\rho_{N,0}/\rho_1 = 0.1$ $\gamma = 5/3$ $c_{s,1}/v_0 = 1.5$
Mach number
$\eta = x\ k/v_0$
$v_1 < v_0 < c_{s,1}$
$v_0 < v_1 < c_{s,1}$
$v_0 < c_{s,1} < v_1$

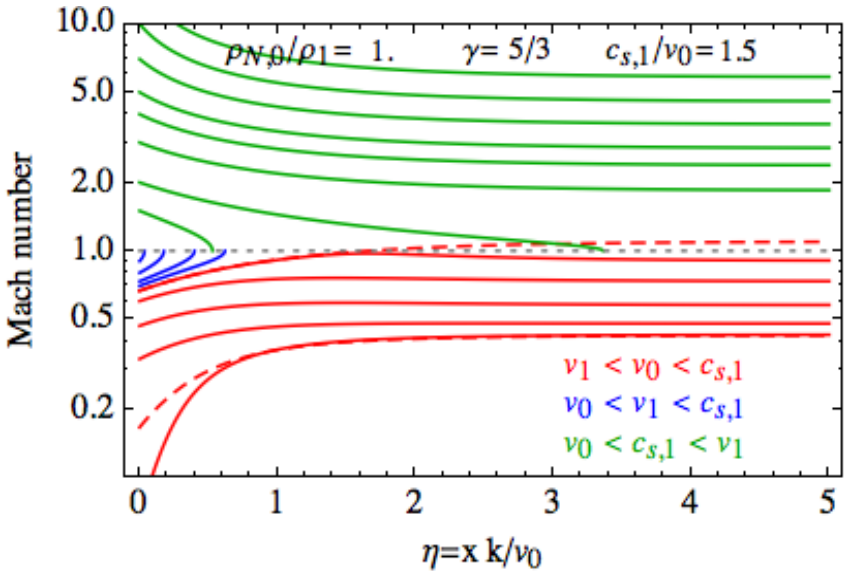
$\rho_{N,0}/\rho_1 = 1.$ $\gamma = 5/3$ $c_{s,1}/v_0 = 1.5$
Mach number
$\eta = x\ k/v_0$
$v_1 < v_0 < c_{s,1}$
$v_0 < v_1 < c_{s,1}$
$v_0 < c_{s,1} < v_1$

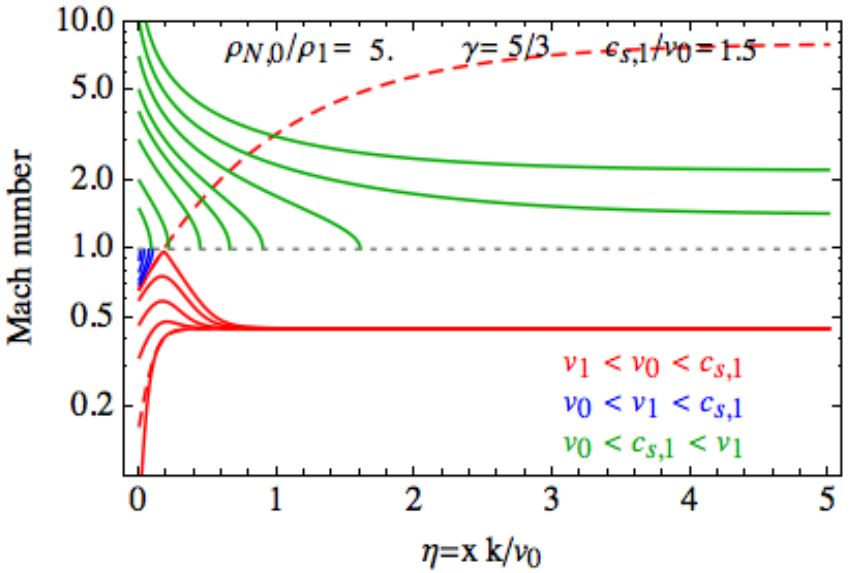
$\rho_{N,0}/\rho_1 = 5.$ $\gamma = 5/3$ $c_{s,1}/v_0 = 1.5$
Mach number
$\eta = x\ k/v_0$
$v_1 < v_0 < c_{s,1}$
$v_0 < v_1 < c_{s,1}$
$v_0 < c_{s,1} < v_1$

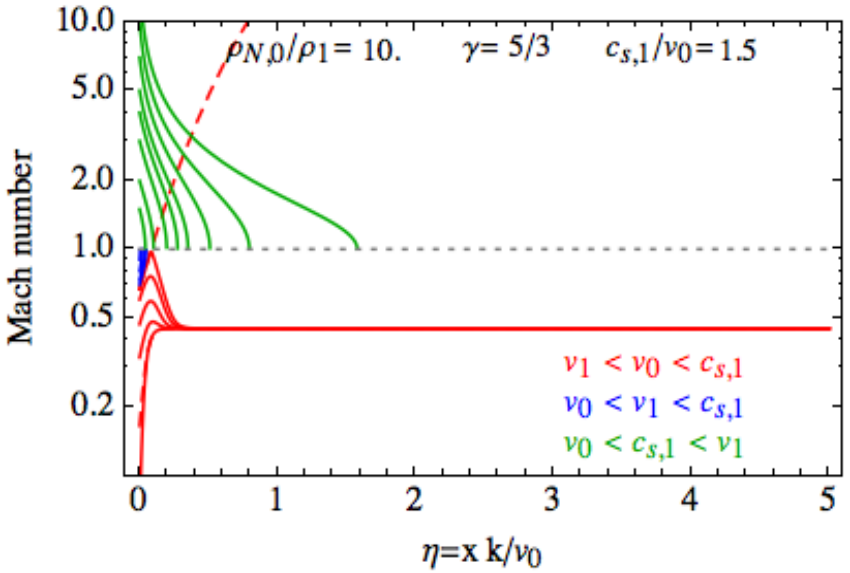
$\rho_{N,0}/\rho_1 = 10.$ $\gamma = 5/3$ $c_{s,1}/v_0 = 1.5$
Mach number
$\eta = x\ k/v_0$
$v_1 < v_0 < c_{s,1}$
$v_0 < v_1 < c_{s,1}$
$v_0 < c_{s,1} < v_1$